

In situ axion generation and detection in laser-driven wakefields

Xiangyan An,^{1,2,3} Min Chen,^{2,3,*} Jianglai Liu,^{1,†} Zhan Bai,^{4,5}
Liangliang Ji,^{4,5} Zhengming Sheng,^{2,1,3} and Jie Zhang^{2,1,3}

¹State Key Laboratory of Dark Matter Physics, Tsung-Dao Lee Institute,
Shanghai Jiao Tong University, Shanghai 201210, China

²State Key Laboratory of Dark Matter Physics, Key Laboratory for Laser Plasmas (MoE),
School of Physics and Astronomy, Shanghai Jiao Tong University, Shanghai 200240, China

³Collaborative Innovation Center of IFSA, Shanghai Jiao Tong University, Shanghai 200240, China

⁴State Key Laboratory of High Field Laser Physics,
Shanghai Institute of Optics and Fine Mechanics, Chinese Academy of Sciences

⁵CAS Center for Excellence in Ultra-intense Laser Science

(Dated: April 18, 2025)

We propose a laser-plasma wakefield based schemes for in situ axion generation and detection through the Primakoff process. Strong electromagnetic fields ($\gtrsim 10^9$ V/cm) in the wakefield enhance axion production rates by orders of magnitude compared to conventional light-shining-through-wall (LSW) experiments. By replacing the axion generation stage with laser-wakefield interaction, one can achieve the axion-photon coupling constraints to the level of $g_{a\gamma\gamma} \sim 10^{-12}$ GeV⁻¹. Besides, the generated axions can convert back into photons in the background field, leading to axion-regenerated electromagnetic fields (AREM) with unique polarization, frequency, and transverse distribution properties. This allows for effective filtering of the AREM from the background field, enhancing signal-to-noise ratios. This approach establishes plasma wakefields as a promising platform for laboratory axion searches.

Introduction: The axion, a hypothetical pseudoscalar particle proposed to resolve the strong CP problem in quantum chromodynamics (QCD) [1–3], has garnered significant attention as a prime candidate for cold dark matter [4–7]. Emerging from the spontaneous breaking of the Peccei-Quinn (PQ) symmetry, axions and axion-like particles (ALPs) offer a natural extension to the Standard Model (SM), with their coupling to photons ($g_{a\gamma\gamma}$) inversely related to their mass (m_a) in generic models [8–13]. Beyond solving fundamental particle physics puzzles, axions are also predicted to permeate the universe as dark matter, driving extensive experimental efforts to detect their feeble interactions with electromagnetic fields.

Conventional axion searches rely on electromagnetic coupling effects. Haloscope experiments exploit resonant cavities to convert galactic axions into microwave photons under strong magnetic fields [14–16], while helioscopes aim to detect solar axions via X-ray production in magnetic setups [17, 18]. Laboratory-based approaches, such as “light-shining-through-wall” experiments [19–24], employ lasers and magnetic fields to generate axions, which subsequently traverse a barrier and recon-vert into detectable photons. Polarization-based methods, including vacuum birefringence measurements (e.g., PVLAS), further probe axion-induced modifications to photon propagation [25–28]. However, these techniques face critical bottlenecks that the axion-photon coupling is extraordinarily weak, demanding both extreme magnetic field strengths and long interaction lengths to achieve detectable signals.

Recent breakthroughs in laser-plasma physics present a possible alternative for axion generation and detection. In laser-driven plasmas, wakefield acceleration gen-

erates quasi-static electric fields exceeding 10^9 V/cm [29–32], surpassing the equivalent fields of state-of-the-art magnets by two orders of magnitude. These fields arise from charge separation in the plasma, providing a robust environment for axion production via the Primakoff effect. Furthermore, plasma channels enable guided propagation of intense laser pulses over centimeter-to-meter scales [33–37], circumventing diffraction limits and significantly extending the interaction length compared to free-space laser propagation. This combination of ultra-high fields and sustained propagation addresses the critical challenge of low axion yield in conventional experiments.

Based on integrating axion electrodynamics in the particle-in-cell code EPOCH [38, 39], this work proposes a novel way for in situ axion generation and conversion in laser-driven wakefields. We demonstrate self-consistently that the strong laser fields in plasma wakefields can induce axion production via the Primakoff effect, with the generated axions subsequently converting back into photons in the background field. Not only the strong wakefields can enhance the axion production rate, but also the AREM would show unique signatures, which would help the detection of axions.

Axion generation and the correlated secondary EM field: Figure 1 illustrates the proposed scheme for wakefield based axion generation and detection (WBAG&D). An intense laser pulse is injected into a plasma to excite and surf in the wakefield. The laser field would couple with the wakefield to generate axions via the Primakoff effect. Meanwhile, the generated axions would also convert back into photons in the background field, which would be treated as the fields AREM \mathbf{E}_1 , \mathbf{B}_1 in our model

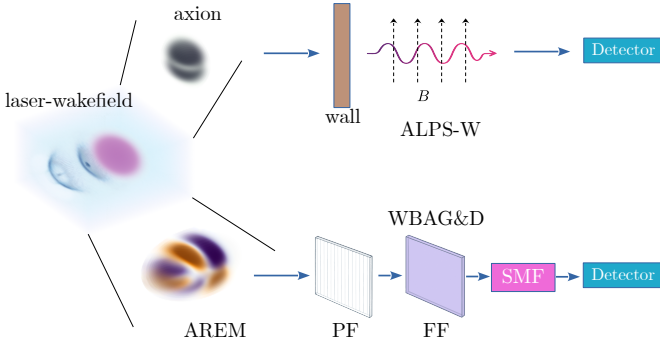


Figure 1. Schematic of axion generation and detection in laser-wakefield interactions. In ALPS-W, one can replace the generation stage of ALPS [20] with the laser-wakefield interaction. In WBAG&D, the polarization filter (PF), frequency filter (FF), and spatial mode filter (SMF) are used to help detect the AREM.

and simulation [39].

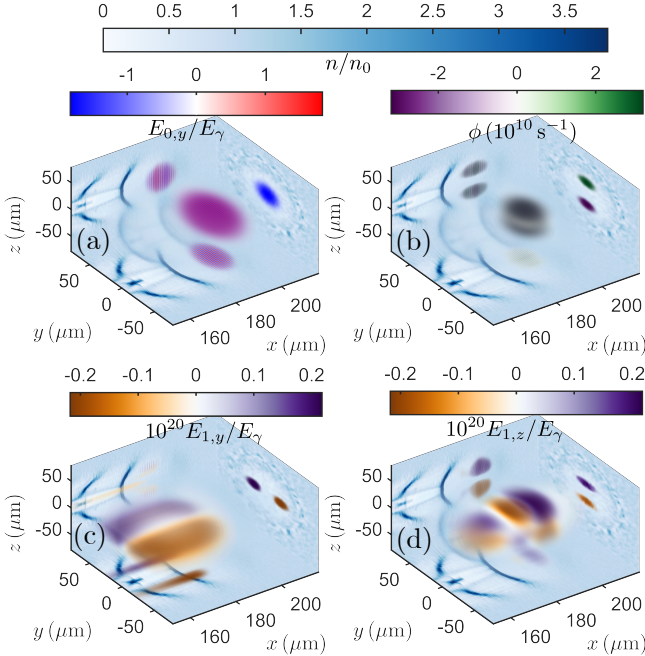


Figure 2. Typical results of axion generation and conversion through laser-wakefield interactions. Different fields with the plasma wakefield are shown: (a) the laser electric field $E_{0,y}$, (b) the axion field ϕ , (c) the AREM $E_{1,y}$, and (d) the AREM $E_{1,z}$. The electric fields are normalized to the characteristic field E_{γ} at the laser frequency.

As a typical example, we consider using a laser with a wavelength of $\lambda_0 = 800$ nm and a normalized amplitude $a_0 = E_0/E_{\gamma} = 5$, where $E_{\gamma} = |m_e \omega_0 c/e|$, $\omega_0 = ck_0 = 2\pi c/\lambda_0$ is the angular frequency. The laser pulse carries Gaussian envelopes in both longitudinal and transverse directions. The longitudinal duration is $12\tau_0 = 24\pi/\omega_0$, while the transverse duration is $w_{\perp} = 50\lambda_0$. The simu-

lation results by using the axion-included PIC code are shown in Fig. 2. The axion field carries a similar envelope as the laser pulse. Therefore, to reduce the divergence of the axion pulse in the long distance interaction, we had used a large laser spot size. The plasma density is set as $n_e = n_0 + \delta n r_{\perp}^2$, where $n_0 = 0.003n_c$, $n_c = \varepsilon_0 m_e \omega_0^2/e^2$ is the critical plasma density, $\delta n = 4\varepsilon_0 m_e c^2/(e^2/w_{\perp}^4)$ is the plasma channel depth which matches the laser width.

As for the axion, the typical parameters we considered are $m_a = m_{\text{sample}} = 10^{-6}$ eV and $g_{a\gamma\gamma} = g_{\text{sample}} = 10^{-9}$ GeV $^{-1}$. In this manuscript, we would focus on the properties of the axion and AREM generated in the laser-wakefield interaction. The plasma effect on the AREM during propagation is left in the future work. Therefore, in this work the effect of different $g_{a\gamma\gamma}$ is clear that the axion field $\phi \propto g_{a\gamma\gamma}$ and the AREM $\mathbf{E}_1 \propto g_{a\gamma\gamma}^2$. Only one typical $g_{a\gamma\gamma}$ is needed to show the properties of the axion field and AREM. Moreover, a larger axion mass (close to the photon energy) may lead to the axion-photon phase-mismatching, and we will discuss it later in this manuscript.

As shown in [39–41], the axion generation and AREM conversion can be described by the modified Maxwell's equations (using natural units $\hbar = c = \varepsilon_0 = 1$ from now on):

$$(\partial_t^2 - \nabla^2 + m_a^2) \phi = g_{a\gamma\gamma} \mathbf{E} \cdot \mathbf{B}, \quad (1)$$

$$\nabla \times \mathbf{E}_1 = -\partial_t \mathbf{B}_1, \quad (2)$$

$$\nabla \times \mathbf{B}_1 = \partial_t \mathbf{E}_1 + g_{a\gamma\gamma} [(\partial_t \phi) \mathbf{B}_0 - \mathbf{E}_0 \times \nabla \phi], \quad (3)$$

where \mathbf{E}_0 and \mathbf{B}_0 are the electromagnetic fields without the axion, and \mathbf{E}_1 and \mathbf{B}_1 are the AREM. Since the axion coupling is sufficiently weak, the AREM can be treated as a perturbation to background field. Thus, we can treat \mathbf{E}_1 and \mathbf{B}_1 independently in the analysis and simulations.

To describe the axion and AREM generation, we would describe the laser field as:

$$\mathbf{E}_y = \frac{a_0}{2} \mathcal{F}_{\gamma}(\zeta_0, y, z) e^{i\zeta_0} + \text{c.c.}, \quad (4)$$

$$\mathbf{B}_z = \frac{a_0 k_0}{2\omega_0} \mathcal{F}_{\gamma}(\zeta_0, y, z) e^{i\zeta_0} + \text{c.c.}, \quad (5)$$

where c.c. means the complex conjugation, $\zeta_0 = k_0 x - \omega_0 t$ is the laser phase, $\mathcal{F}_{\gamma}(\zeta_0, y, z) = \exp(-\zeta_0^2/w_l^2 - (y^2 + z^2)/w_{\perp}^2)$ is the laser envelope, $\zeta_0 = x - v_g t$ is the moving coordinate, v_g is the laser group velocity, w_l and w_{\perp} are the longitudinal and transverse spot size, respectively, and a_0 is the normalized amplitude. The normalized wakefield can be phenomenologically described as [42, 43]:

$$E_x = \frac{k_p \zeta_0}{2} \frac{\omega_p}{\omega_0}, \quad E_y = -B_z = \frac{k_p y}{4} \frac{\omega_p}{\omega_0}, \quad (6)$$

$$B_x = 0, \quad E_z = B_y = \frac{k_p z}{4} \frac{\omega_p}{\omega_0}. \quad (7)$$

For the simulation results, we can assume the axion field ϕ and the vector potential \mathbf{A}_1 of the AREM both

have the same envelope as each one's source, then the axion field and AREM can be analytically derived as:

$$\phi = -\frac{2\mathcal{F}_a(\zeta_0, y, z)}{k_a \kappa} \sin(\kappa x/2) \sin(\xi_a + \kappa x/2), \quad (8)$$

$$A_{1,y} = -\frac{g_{a\gamma\gamma}\mathcal{F}_a}{k_a \kappa k^{(1)} \kappa'_1 \omega_0} (k_a + \omega_a) \omega_p k_p z \sin(\kappa x/2) \sin(\kappa'_1 x/2) \sin(\xi_1^{(1)} + \kappa'_1 x/2), \quad (9)$$

$$A_{1,z} = -\frac{g_{a\gamma\gamma}\mathcal{F}_a}{k_a \kappa \omega_0} \sin(\kappa x/2) \left[\frac{(k_a + \omega_a)}{k^{(1)} \kappa'_1} \omega_p k_p y \sin(\kappa'_1 x/2) \sin(\xi_1^{(1)} + \kappa'_1 x/2) - 2a_0 \mathcal{F}_\gamma \kappa \omega_0 \left(\frac{\sin(\kappa'_0 x/2) \sin(\xi_0^{(1)} + \kappa'_0 x/2)}{k_0^{(1)} \kappa'_0} + \frac{\sin(\kappa'_2 x/2) \sin(\xi_2^{(1)} + \kappa'_2 x/2)}{k_2^{(1)} \kappa'_2} \right) \right], \quad (10)$$

where $\mathcal{F}_a(\zeta_0, y, z) = g_{a\gamma\gamma} a_0 \omega_p k_p z \mathcal{F}_\gamma / (4\omega_0)$ is the envelope of the axion field, $\xi_a = k_a x - \omega_a t \approx \xi_0$ is the axion field phase, $\xi_\mu^{(1)} = k_\mu^{(1)} x - \omega_\mu^{(1)} t$ is the AREM phase, and $\kappa = k_0 - k_a$, $\kappa'_\mu = k_\mu^{(s)} - k_\mu^{(1)} + \kappa/2$. Here the superscript (1) and (s) label the variables of the AREM and their source, respectively. The subscript $\mu = 0, 1, 2$ labels the different frequency components: $\omega_\mu^{(1)} = \mu\omega_0$, $k_\mu^{(s)} = k_a - k_0$, k_a , $k_a + k_0$, respectively. (See the supplemental material [44] for details of derivation).

Although the axion field is mainly at the laser frequency, the AREM would have multiple frequency components. The components at 0 and $2\omega_0$ resulted from the coupling between the axion field and the intense laser. In our scheme, not only the strong wakefield can provide a strong background field to enhance the direct axion generation, but also the axion would couple with the laser field to generate a non-trivial AREM. Such an advantage is not available in the ALPS experiments.

Since the wakefield exhibits a cylindrically symmetric structure with a longitudinal electric field and an azimuthal magnetic field, and the injected laser pulse is polarized along the y direction, the generated axion field would be inverse in the $y > 0$ and $y < 0$ regions. Such a transverse profile would be inherited by the AREM. Therefore, besides the characteristic frequencies in the AREM, we can also see that the AREM show special transverse profiles. To describe the transverse profile, we can decompose on the Laguerre-Gaussian (LG) modes:

$$u_{pl} = a_{pl} \frac{1}{w_\perp} \left(\frac{\sqrt{2}r_\perp}{w_\perp} \right)^{|l|} L_p^{|l|} \left(\frac{2r_\perp^2}{w_\perp^2} \right) e^{-r_\perp^2/w_\perp^2} e^{-il\theta}, \quad (11)$$

where $a_{pl} = \sqrt{\frac{2p!}{\pi(p+|l|)!}}$ is the normalization factor, $L_p^{|l|}$ is the generalized Laguerre polynomial, and l and p are the azimuthal and radial indices, respectively. The LG decomposition of a field E can be obtained by: $C_{pl} =$

$$\int_0^{2\pi} d\theta \int_0^\infty r_\perp dr_\perp u_{pl}^* E(r_\perp, \theta).$$

According to the results in Eqs. (8-10), We can obtain the LG decomposition of the different components of the AREM:

$$A_{1,y,\omega_0} : C_{pl} \neq 0 \quad \text{only when } l = 0, \pm 2, \quad (12)$$

$$A_{1,z,0\omega_0} : C_{pl} \neq 0 \quad \text{only when } l = \pm 1, \quad (13)$$

$$A_{1,z,\omega_0} : C_{pl} \neq 0 \quad \text{only when } l = \pm 2, \quad (14)$$

$$A_{1,z,2\omega_0} : C_{pl} \neq 0 \quad \text{only when } l = \pm 1. \quad (15)$$

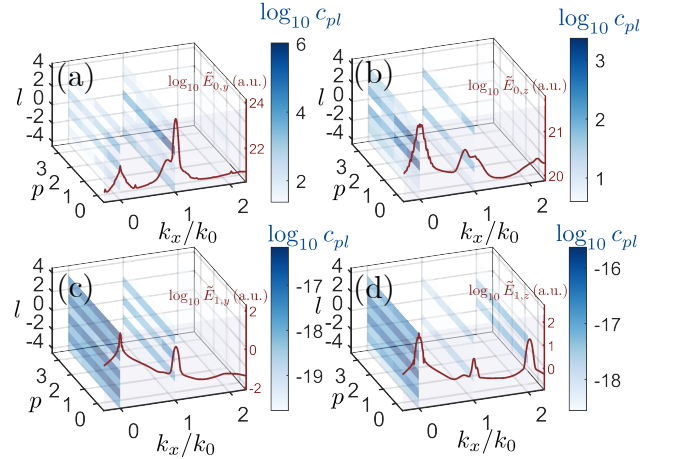


Figure 3. Frequency and LG decomposition of different field components: (a) $E_{0,y}$, (b) $E_{0,z}$, (c) $E_{1,y}$, and (d) $E_{1,z}$. The red lines show the frequency spectrums. The slices at different frequencies show the LG decomposition of the corresponding frequency components.

For the simulation results, we made Fourier transform on the AREM and then filtered out the components at different frequencies. The results are shown in Fig. 3. According to the simulation results, we can find that the AREM do have specific frequency and LG components, which match the theoretical analysis. Moreover,

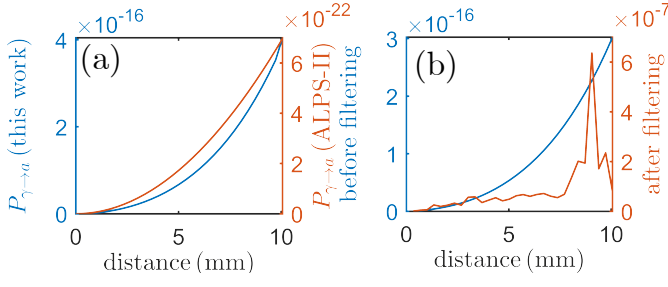


Figure 4. (a) Axion conversion ratio in this work and ALPS-II experiment. (b) The signal-to-noise ratio before filtering ($E_{1,y}/E_{0,y}$) and after filtering ($E_{1,z,2\omega_0,l=1}/E_{0,z,2\omega_0,l=1}$).

Although the exact coefficients of the LG modes at different p are hard to derived theoretically, they can be provided by the simulation results. All the components contain multiple p modes, because the AREM transverse profile is no longer the injected laser profile after multiple interactions, which would resulted in a non-zeros result when making the integral of LG decomposition.

Long distance interaction and discussion: Comparing with the traditional LSW experiment, the AREM here propagate together with the laser and axion, which makes it hard to distinguish them from the background field. Since the AREM show unique properties on the polarization, frequency, and transverse modes, we can filter the whole field in these ways to reduce the background field and keep the AREM not strongly affected. By this means, the signal (AREM E_1) to noise (E_0) ratio can be significantly enhanced. The polarization and frequency filter are quite well-established. Meanwhile, there are also LG mode sorters proposed to decompose a beam into a Cartesian grid of identical Gaussian spots each containing a single Laguerre-Gaussian component [45], which may serve as the spatial mode filter needed in our scheme.

Unfortunately, the effectiveness of background field E_0 filtering strongly depends on the transverse resolution of the simulation (See the supplemental material [44] for details). However, a simulation with both high transverse resolution and long interaction length (1 cm) is quite a challenge. As a compromise, in the long distance simulation, the wakefield is artificially set as Eqs. (6-7) rather than generated by the plasma.

Figure 4(a) shows the axion conversion ratio, comparing with the ALPS-II experiment [20]. The conversion ratio in this work is much higher than the ALPS-II experiment, which is mainly due to the strong wakefield. Here an effective magnetic field of $B_{\text{eff}} \approx 4000$ T is achieved in the highly nonlinear wakefield, where the electric and magnetic fields in the wakefield share the same contributions. Even if we take the interaction distance into account (with the parameter $Bl = 468$ T·m), the conversion ratio in ALPS-II experiment could be 7.7×10^{-14} , while the conversion ratio in this work could be 4.0×10^{-12}

(considering a reasonable laser guiding length as 1 m). Therefore, due to the strong wakefield, the axion generation can be more efficient in the laser-wakefield interaction, which makes the axion detection more efficient if one replaces the first section of the LSW experiment with the laser-wakefield interaction. In another way, the AREM is also possible to be detected directly. Recently, high power lasers have been successfully guided by the plasma channel in the meter scale distance [33–36]. To guide the laser in the 10 m to 1 km distances may also be possible in the future. In such a case, the AREM could be strong enough on its own. Then it would be possible to detect the AREM solely by filtering all the background field. Here we illustrate the effect of filtering based on the properties of the AREM and background fields. Such a scheme can be applied when the laser is guided in the long distance and AREM is strong enough. Figure 4(b) shows the signal-to-noise ratio (the ratio between the AREM E_1 and the background field E_0) before and after filtering. One can see that the AREM E_1 also increases by square with the distance. Besides, the filtering can reduce the noise significantly, which makes the AREM detection feasible.

In the regime of long-distance interactions, the axion mass may give rise to the phase-mismatching issue, which need to be taken into account. As shown in Eqs. (8-10), the phase mismatching issue comes from the broken approximation of $\sin(\kappa x/2) \sim \kappa x/2$. Therefore, to avoid the reduction of the axion and AREM generation, the interaction length is limited in $x \lesssim l_d \equiv 2\pi/|\kappa|$ and $x \lesssim l'_d \equiv 2\pi/|\kappa'|$, where l_d and l'_d are two dephasing distances of the axion and AREM, respectively.

Notice that to calculate the dephasing distances, we need to consider the laser wave number k_0 . In a uniform plasma, it's given by the dispersion relationship $\omega_0^2 = \omega_p^2 + k_0^2$, and the plasma density n_0 is needed. However, due to the electron exclusion from the bubble by the laser pulse and relativistic correction, the electron density felt by the laser pulse is in fact less than the initial background density. According to the simulation results, the electron density in the bubble is approximately $n_{\text{eff}} \approx 0.3n_0$. Thus, the effective plasma frequency is $\omega_{p,\text{eff}}^2 = n_{\text{eff}}e^2/(\gamma_{\perp}m_e)$, $\gamma_{\perp} = \sqrt{1 + a_0^2/2} = 3.7$.

Then we can obtain: $\kappa = \sqrt{\omega_0^2 - \omega_{p,\text{eff}}^2} - \sqrt{\omega_0^2 - m_a^2}$, and $\kappa' = \frac{1}{2}\sqrt{\omega_0^2 - m_a^2} + \frac{3}{2}\sqrt{\omega_0^2 - \omega_{p,\text{eff}}^2} - \sqrt{4\omega_0^2 - \omega_{p,\text{eff}}^2}$. Notice that $\kappa = 0$ can be achieved as long as $m_a = \omega_{p,\text{eff}}$, meaning that there is no phase-mismatching issue at all. Moreover, as $m_a \rightarrow 0$, κ and κ' would tend to the same limit $|\kappa| \approx |\kappa'| \approx \frac{1}{2}\frac{\omega_{p,\text{eff}}^2}{\omega_0}$, which is decided by the effective plasma density in the wakefield bubble. Therefore, the remained electrons in the bubble might limit the axion and AREM generation in the long distance interaction. However, if the wakefield is driven by a relativistic electron beam, the bubble could be much

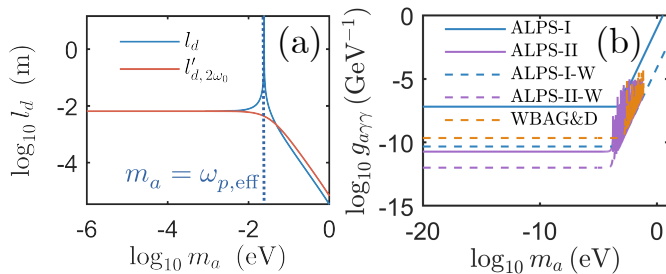


Figure 5. (a) The dephasing distances of the axion and AREM. (b) The axion-photon coupling constraint that can be achieved in this work. The solid lines show the constraints from the ALPS experiments [46], while the dashed lines show the constraints by replacing the generation stage of the ALPS experiments with the laser-wakefield interaction (indicated by ALPS-I/II-W).

cleaner than the laser-driven wakefield. In this case, the effective plasma frequency would be small enough to make the dephasing distances large enough (See the supplemental material [44]). For example, in the beam-driven wakefield, the bubble remained density could be $n_{eff} < 0.01n_0$ and the corresponding effective plasma frequency is $\omega_{p,eff} < 2.3$ meV. Then the dephasing distances at $m_a \rightarrow 0$ would be $l_d \approx l'_d > 0.7$ m, which is long enough for a 1-meter laser-wakefield interaction.

In general, since the axion generation ratio is higher than the ALPS experiments due to the strong wakefield ($P_a(g_{sample}) \propto (g_{sample}Bl)^2$), one can get a higher axion generation ratio if one replaces the generation stage of the ALPS experiments with the laser-wakefield interaction. Besides the axion generation ratio, the effective photon number can also be higher. Compared with the effective laser power 150 kW in ALPS-II [20], the effective power P_{laser} of a 1 PW laser running on 1 Hz repetition frequency and 1 m interaction distance could be 3 MW. Both the higher effective laser power and axion generation ratio could amplify the axion generation number. This intensified production mechanism implies that substituting the generation stage of ALPS experiments with wakefield-driven systems could substantially improve detection sensitivity. With the same detection setups, the bound on the axion-photon coupling constants $g_{a\gamma\gamma}$ could be limited to a lower value ($g_{a\gamma\gamma} \propto P_{laser}^{-1/4} P_a^{-1/2}(g_{sample})$). The improvements of the ALPS experiments by replacing the generation stage are shown in Fig. 5(b). The solid lines show the constraints from the ALPS experiments, while the dashed lines show the constraints by replacing the generation stage with the laser-wakefield interaction.

Besides simply replacing the generation stage, we also proposed to detect the AREM simultaneously generated in the wakefield. Such a signal is ultra weak, but the ratio can be enhanced by the filtering according to the unique properties of the AREM (polarization, frequency, and LG

modes). By assuming the interaction length to be 1 m and an acceptable final detection efficiency of 10^{-4} , the axion-photon coupling constraint that can be achieved in this work is shown in Fig. 5(b). It is close to the replacement of ALPS-I experiment, and also better than the current ground-based laboratory experiments.

Summary: In this work, we have proposed a novel platform for in situ axion generation and conversion in laser-driven wakefields. The strong laser fields in plasma wakefields can induce axion production via the Primakoff effect, with the generated axions subsequently converting back into photons in both the laser and wakefield. The axion field and AREM show unique properties on the polarization, frequency, and transverse distribution, which can be used to filter the AREM from the background field. The axion generation ratio is much higher than the ALPS experiments due to the strong wakefield. By replacing the generation stage of ALPS experiments with the laser-wakefield interaction, one can achieve a better axion-photon coupling constraint. Moreover, by detecting the AREM simultaneously generated in the wakefield, one can also achieve a better axion-photon coupling constraint than the current ground-based laboratory experiments.

ACKNOWLEDGMENTS

The computations in this paper were run on the π 2.0 cluster supported by the Center for High Performance Computing at Shanghai Jiao Tong University. This work was supported by the National Natural Science Foundation of China (Grants No. 12225505).

* minchen@sjtu.edu.cn

† jianglai.liu@sjtu.edu.cn

- [1] F. Wilczek, Problem of strong P and T invariance in the presence of instantons, *Phys. Rev. Lett.* **40**, 279 (1978).
- [2] S. Weinberg, A new light boson?, *Phys. Rev. Lett.* **40**, 223 (1978).
- [3] J. E. Kim and G. Carosi, Axions and the strong CP problem, *Rev. Modern Phys.* **82**, 557 (2010).
- [4] J. Preskill, M. B. Wise, and F. Wilczek, Cosmology of the Invisible Axion, *Phys. Lett. B* **120**, 127 (1983).
- [5] L. F. Abbott and P. Sikivie, A Cosmological Bound on the Invisible Axion, *Phys. Lett. B* **120**, 133 (1983).
- [6] M. Dine and W. Fischler, The Not So Harmless Axion, *Phys. Lett. B* **120**, 137 (1983).
- [7] D. J. E. Marsh, Axion Cosmology, *Phys. Rept.* **643**, 1 (2016).
- [8] P. Svrcek and E. Witten, Axions in string theory, *J. High Energy Phys.* **2006** (6), 51.
- [9] G. B. Gelmini and M. Roncadelli, Left-Handed Neutrino Mass Scale and Spontaneously Broken Lepton Number, *Phys. Lett. B* **99**, 411 (1981).

- [10] B. Bellazzini, A. Mariotti, D. Redigolo, F. Sala, and J. Serra, *R-axion at colliders*, *Phys. Rev. Lett.* **119**, 141804 (2017).
- [11] Y. Ema, K. Hamaguchi, T. Moroi, and K. Nakayama, *Flaxion: a minimal extension to solve puzzles in the standard model*, *J. High Energy Phys.* **2017** (1), 96.
- [12] L. Calibbi, F. Goertz, D. Redigolo, R. Ziegler, and J. Zupan, *Minimal axion model from flavor*, *Phys. Rev. D* **95**, 095009 (2017).
- [13] I. G. Irastorza and J. Redondo, *New experimental approaches in the search for axion-like particles*, *Prog. Part. Nucl. Phys.* **102**, 89 (2018).
- [14] J. E. Kim, *Weak Interaction Singlet and Strong CP Invariance*, *Phys. Rev. Lett.* **43**, 103 (1979).
- [15] M. A. Shifman, A. I. Vainshtein, and V. I. Zakharov, *Can Confinement Ensure Natural CP Invariance of Strong Interactions?*, *Nucl. Phys. B* **166**, 493 (1980).
- [16] M. Dine, W. Fischler, and M. Srednicki, *A Simple Solution to the Strong CP Problem with a Harmless Axion*, *Phys. Lett. B* **104**, 199 (1981).
- [17] CAST Collaboration, *New CAST limit on the axion–photon interaction*, *Nat. Phys.* **13**, 584 (2017).
- [18] E. Armengaud *et al.*, *Physics potential of the international axion observatory (IAXO)*, *J. Cosmol. Astropart. Phys.* **2019** (6), 47.
- [19] K. Ehret, M. Frede, S. Ghazaryan, M. Hildebrandt, E.-A. Knabbe, D. Kracht, A. Lindner, J. List, T. Meier, N. Meyer, D. Notz, J. Redondo, A. Ringwald, G. Wiedemann, and B. Willke, *New ALPS results on hidden-sector lightweights*, *Phys. Lett. B* **689**, 149 (2010).
- [20] R. Bähre *et al.*, *Any light particle search II — technical design report*, *J. Instrum.* **8** (9), T09001.
- [21] A. S. Chou, W. Wester, A. Baumbaugh, H. R. Gustafson, Y. Irizarry-Valle, P. O. Mazur, J. H. Steffen, R. Tomlin, X. Yang, and J. Yoo, *Search for axionlike particles using a variable-baseline photon-regeneration technique*, *Phys. Rev. Lett.* **100**, 80402 (2008).
- [22] A. Afanasev, O. K. Baker, K. B. Beard, G. Biallas, J. Boyce, M. Minarni, R. Ramdon, M. Shinn, and P. Slocum, *Experimental Limit on Optical-Photon Coupling to Light Neutral Scalar Bosons*, *Phys. Rev. Lett.* **101**, 120401 (2008).
- [23] P. Pognat, L. Duvillaret, R. Jost, G. Vitrant, D. Romanini, A. Siemko, R. Ballou, B. Barbara, M. Finger, M. Finger, J. Hošek, M. Král, K. A. Meissner, M. Šulc, and J. Zicha, *Results from the OSQAR photon-regeneration experiment: No light shining through a wall*, *Phys. Rev. D* **78**, 92003 (2008).
- [24] C. Robilliard, R. Battesti, M. Fouché, J. Mauchain, A.-M. Sautivet, F. Amiranoff, and C. Rizzo, *No “Light Shining through a Wall”: Results from a Photoregeneration Experiment*, *Phys. Rev. Lett.* **99**, 190403 (2007).
- [25] A. Ejlli, F. Della Valle, U. Gastaldi, G. Messineo, R. Pengo, G. Ruoso, and G. Zavattini, *The PVLAS experiment: a 25 year effort to measure vacuum magnetic birefringence*, *Phys. Rep.* **871**, 1 (2020).
- [26] R. Battesti, B. Pinto Da Souza, S. Batut, C. Robilliard, G. Bailly, C. Michel, M. Nardone, L. Pinard, O. Portugall, G. Tréneç, J.-M. Mackowski, G. L. Rikken, J. Vigué, and C. Rizzo, *The BMV experiment: a novel apparatus to study the propagation of light in a transverse magnetic field*, *Eur. Phys. J. D* **46**, 323 (2008).
- [27] R. Cameron, G. Cantatore, A. Melissinos, G. Ruoso, Y. Semertzidis, H. Halama, D. Lazarus, A. Prodell, F. Nezzrick, C. Rizzo, and E. Zavattini, *Search for nearly massless, weakly coupled particles by optical techniques*, *Phys. Rev. D* **47**, 3707 (1993).
- [28] S.-J. Chen, H.-H. Mei, and W.-T. Ni, *Q & a experiment to search for vacuum dichroism, pseudoscalar–photon interaction and millicharged fermions*, *Mod. Phys. Lett. A* **22**, 2815 (2007).
- [29] E. Esarey, C. B. Schroeder, and W. P. Leemans, *Physics of laser-driven plasma-based electron accelerators*, *Rev. Modern Phys.* **81**, 1229 (2009).
- [30] S. P. D. Mangles, C. D. Murphy, Z. Najmudin, A. G. R. Thomas, J. L. Collier, A. E. Dangor, E. J. Divall, P. S. Foster, J. G. Gallacher, C. J. Hooker, D. A. Jaroszynski, A. J. Langley, W. B. Mori, P. A. Norreys, F. S. Tsung, R. Viskup, B. R. Walton, and K. Krushelnick, *Monoenergetic beams of relativistic electrons from intense laser–plasma interactions*, *Nature* **431**, 535 (2004).
- [31] C. G. R. Geddes, C. Toth, J. Van Tilborg, E. Esarey, C. B. Schroeder, D. Bruhwiler, C. Nieter, J. Cary, and W. P. Leemans, *High-quality electron beams from a laser wakefield accelerator using plasma-channel guiding*, *Nature* **431**, 538 (2004).
- [32] J. Faure, Y. Glinec, A. Pukhov, S. Kiselev, S. Gordienko, E. Lefebvre, J.-P. Rousseau, F. Burgy, and V. Malka, *A laser–plasma accelerator producing monoenergetic electron beams*, *Nature* **431**, 541 (2004).
- [33] B. Miao, L. Feder, J. Shrock, A. Goffin, and H. Milchberg, *Optical Guiding in Meter-Scale Plasma Waveguides*, *Phys. Rev. Lett.* **125**, 074801 (2020).
- [34] A. Picksley, J. Stackhouse, C. Benedetti, K. Nakamura, H. Tsai, R. Li, B. Miao, J. Shrock, E. Rockafellow, H. Milchberg, C. Schroeder, J. van Tilborg, E. Esarey, C. Geddes, and A. Gonsalves, *Matched guiding and controlled injection in dark-current-free, 10-GeV-class, channel-guided laser-plasma accelerators*, *Phys. Rev. Lett.* **133**, 255001 (2024), publisher: American Physical Society.
- [35] B. Miao, E. Rockafellow, J. Shrock, S. Hancock, D. Gordon, and H. Milchberg, *Benchmarking of hydrodynamic plasma waveguides for multi-GeV laser-driven electron acceleration*, *Phys. Rev. Accel. Beams* **27**, 81302 (2024).
- [36] J. Shrock, E. Rockafellow, B. Miao, M. Le, R. Hollinger, S. Wang, A. Gonsalves, A. Picksley, J. Rocca, and H. Milchberg, *Guided mode evolution and ionization injection in meter-scale multi-GeV laser wakefield accelerators*, *Phys. Rev. Lett.* **133**, 45002 (2024), publisher: American Physical Society.
- [37] X. Zhu, B. Li, F. Liu, J. Li, Z. Bi, X. Ge, H. Deng, Z. Zhang, P. Cui, L. Lu, W. Yan, X. Yuan, L. Chen, Q. Cao, Z. Liu, Z. Sheng, M. Chen, and J. Zhang, *Experimental Demonstration of Laser Guiding and Wakefield Acceleration in a Curved Plasma Channel*, *Phys. Rev. Lett.* **130**, 215001 (2023).
- [38] T. D. Arber, K. Bennett, C. S. Brady, A. Lawrence-Douglas, M. G. Ramsay, N. J. Sircombe, P. Gillies, R. G. Evans, H. Schmitz, A. R. Bell, and C. P. Ridgers, *Contemporary particle-in-cell approach to laser-plasma modelling*, *Plasma Phys. Control. Fusion* **57**, 113001 (2015).
- [39] X. An, M. Chen, J. Liu, Z. Sheng, and J. Zhang, *Modeling of axion and electromagnetic fields interaction in particle-in-cell simulations*, *Matter Radiat. Extrem.* **9**, 067204 (2024).
- [40] L. Visinelli, *Axion-electromagnetic waves*, *Modern Phys. Lett. A* **28**, 1350162 (2013).

- [41] H. Terças, J. Rodrigues, and J. Mendonça, Axion-Plasmon Polaritons in Strongly Magnetized Plasmas, *Phys. Rev. Lett.* **120**, 181803 (2018).
- [42] I. Kostyukov, A. Pukhov, and S. Kiselev, Phenomenological theory of laser-plasma interaction in “bubble” regime, *Phys. Plasma* **11**, 5256 (2004).
- [43] W. Lu, C. Huang, M. Zhou, W. B. Mori, and T. Katsouleas, Nonlinear Theory for Relativistic Plasma Wakefields in the Blowout Regime, *Phys. Rev. Lett.* **96**, 165002 (2006).
- [44] See Supplemental Material at [URL will be inserted by publisher] for derivation of the axion and AREM generation, comparison of different transverse resolutions, the cleaner wakefield bubble driven by the electron beam, and the estimation based on the extension of the simulation results.
- [45] N. K. Fontaine, R. Ryf, H. Chen, D. T. Neilson, K. Kim, and J. Carpenter, Laguerre-gaussian mode sorter, *Nat. Commun.* **10**, 1865 (2019).
- [46] C. O’Hare, cajohare/axionlimits: Axionlimits, <https://cajohare.github.io/AxionLimits/> (2020).